Applied Thermal Engineering 206 (2022) 118010

Contents lists available at ScienceDirect

Applied Thermal Engineering

journal homepage: www.elsevier.com/locate/apthermeng

Design and test of shape memory alloy fins for self-adaptive liquid cooling device

Desideri Regany [a], Francesc Majós [a], Jérôme Barrau [a], Joan Rosell [a], Manuel Ibáñez [a], Luc G. Fréchette [b], Montse Vilarrubí [a,*]

[a] Dynamic Systems Applied to Solar Energy Research Group, University of Lleida, Lleida, Spain
[b] UMI-LN2, Institut Interdisciplinaire d'Innovation Technologique (3IT), Université de Sherbrooke, Sherbrooke, Canada

ARTICLE INFO

Keywords:
Self-adaptive fins
Liquid cooling
Shape memory alloys
Thermal resistance
Heat transfer enhancement

ABSTRACT

Thermal management complexity increases in high-performance chips, where the heat loads vary spatially and temporally, while liquid cooling systems are usually designed for most stringent stationary conditions. Several works developed heat transfer enhancement techniques to increase the cooling capacity of liquid cooled heat sinks, but pumping power is increased in a permanent way due to the addition of elements within the channels. Here, a liquid cooling self-adaptive heat sink that can efficiently adapt the distribution of its heat extraction capacity to time dependent and non-uniform heat load scenarios is proposed. Numerical design of the mesoscale cooling device with bimorph metal/SMA fins, definition of the fabrication and training procedure of the SMA fins to reach the desired behavior and experimental assessment is presented. The capacity of the self-adaptive fins to locally boost the heat transfer is numerically and experimentally demonstrated. Results obtained show that the self-adaptive fins can improve the temperature uniformity by 63% with respect to plain channel. The reduction in thermal resistance using bimorph metal/SMA fins sample allows the surface maximum temperature gradient to remain almost constant although heat flux increases. Energy savings are maximized in applications where partial load intervals contributes significantly to the overall operating period.

1. Introduction

The continuous increase of power density in electronics, due to the ever-increasing rate of data and communication and the ongoing drive to reduce size and cost, is settling thermal management as a major concern for the industry [1]. Because of the small size and high heat flux density of these systems, compact heat transfer solutions capable of cooling hotspots efficiently while maintaining uniform temperature distributions are required to increase their efficiency and reliability. New cooling solutions should really attempt to minimize associated energy consumption and operating costs.

Liquid cooling is preferred to air cooling when compact and high-power applications are developed, because lower thermal resistances and more compact designs are achieved [2]. However, junction temperature uniformity, which is a key parameter for electronic reliability [3], still remains a challenge. Management complexity increases in high-performance chips like multicore processors [4] and three dimensional integrated circuits (3D-IC), where the heat loads vary spatially and temporally, leading to the appearance of hotspot and background regions and highly non-uniform power map distributions [5,6]. Also, liquid cooling systems are usually designed for most stringent stationary conditions and, as hotspot regions are usually localized, high constant flows through all the cooling device turn on overcooled systems with oversized power consumptions [7–11]. To improve the reliability of cooled electronic devices, a cooling system should tend to give low thermal resistance, as well as spatially uniform and constant wall temperature distributions over time.

Several researches have attempted to overcome this limitation by employing three main strategies: two-phase flow, manifold and matrix designs, and stream-wise customized thermal resistance. Since phase change absorbs heat without causing a temperature rise in the coolant, two-phase flow produces the greatest results for temperature uniformity [12,13]; nevertheless, the challenges in predicting the Critical Heat Flux make this solution problematic [6]. Manifold designs allow inlet coolant to be provided at many locations across the cooled device, improving temperature uniformity while also reducing pressure loss by spreading the flow across multiple short parallel channels. Because a manifold layer must be added above the cooling channel layer, this comes at a cost of complexity [14,15]. In jet impingement cooling systems, a matrix of

* Corresponding author.

https://doi.org/10.1016/j.applthermaleng.2021.118010
Received 30 July 2021; Received in revised form 29 November 2021; Accepted 27 December 2021
Available online 17 January 2022

Nomenclature

A	Surface (m^2)
A_f	SMA austenite finish temperature
A_s	SMA austenite start temperature
C_p	Specific heat (J/kg·K)
D_h	Hydraulic diameter (m)
f	Fanning friction factor (-)
h	Convective heat transfer coefficient ($W/m^2·K$)
H	Height (m)
L	Length (m)
M_f	SMA martensite finish temperature
M_s	SMA martensite start temperature
Nu	Nusselt number (-)
ΔP	Pressure drop (Pa)
p	Perimeter (m)
q''	Heat flux (W/m^2)
Q	Flow rate (m^3/s)
R_{th}	Thermal resistance ($m^2·K/W$)
Re	Reynolds number (-)
T	Temperature (°C)
ΔT	Temperature difference (°C)
TPF	Thermal performance factor (-)
u	Velocity vector (m/s)
v	Velocity (m/s)
W	Width (m)

Greek symbols

β	Angle of attack (°)
κ	Conductive heat transfer coefficient (W/m·K)
μ	Dynamic viscosity (Pa·s)
ρ	Density (kg/m^3)

Subscript

av	Average
base	Solid base of the channel
ch	Channel
chip	Chip
f	Fluid
fin	Solid fin inside cooling channel
OUT	outlet
s	solid

jet nozzles has been used to soften the temperature gradient, which requires a sophisticated hydraulic manifold [16,17].

Barrau et al. [18] and Riera et al. [19] demonstrated the potential of a hybrid jet impingement/microchannel cooling system with variable microchannel width along the flow path to reach low thermal resistances, good temperature uniformities, and low pressure drops for specific heat flux distributions. Also, Vilarrubí et al. [20] presented a variable pin–fin density heat sinks for the dissipation of high heat fluxes from small areas, achieving good results in terms of thermal resistances, surface temperature uniformity and pressure drop. In addition, Sharma et al. [21,22] developed a hotspot-targeted and highly efficient cooling system with optimized microchannel geometry and flow rate distribution. The flow is passively limited in the regions of low heat flux and redirected to the regions with higher heat extraction demands. However, the fixed geometry of the above-mentioned liquid cooling solutions is their principal shortcoming, since the design was developed for a known heat flux and desired temperature distributions. Hence, the heat sink will only offer the correct temperature distribution for specified values of flow rate, coolant inlet temperature, and heat flux distribution, which often correspond to the most critical working conditions. As a result, both thermal non-uniformities and excessive pumping power consumption will appear when conditions change from the design point.

Additionally, to further increase the cooling capacity of liquid cooled heat sinks, several works focused on the development of heat transfer enhancement techniques [23], such as disturbing the thermal boundary layer through flow disruption by using reentrant cavities, porous medium, ribs and grooves structures, fins, vortex generators or rough surfaces, able to create vortices and secondary flows to improve the mixing and heat transfer [24–29]. Fiebig et al. [30,31] analyzed the overall performance of vortex generators within air flow and reported that, for heat transfer enhancement, longitudinal vortex generators were more effective than transverse vortex generators. Also, for identical parameters of study, they reported that delta wings provide more effective cooling than rectangular wings and winglets. The main drawback of these systems is the increase on pressure drop due to the addition of elements within the channel and so, the increment of pumping power in a permanent way.

To overcome the above listed issues, Vilarrubí et al. [32,33] proposed a liquid cooling self-adaptive heat sink that can efficiently adapt the distribution of its heat extraction capacity to time dependent and non-uniform heat load scenarios. In this way, the disturbing elements inside the flow are able to adapt its shape in function of its own temperature [34] and so, the demonstrated capabilities on heat transfer enhancement of flow disturbing elements will only be used when the cooling demands of the device increase; otherwise, the fins will remain in a flat position, reducing the pressure drop and pumping power inside the cooling device.

Previous works validated the *Shape Memory Alloys* (SMA) capability to adapt to time dependent and non-uniform heat load scenarios, although none of them applied to liquid cooled devices. In 2001, Champagne and Bergles [35] presented a novel work using a heat exchanger tube with variable roughness, consisting in SMA wire coils. The heat transfer coefficient was increased between 28% and 64% when the coils were extended, compared to its compressed position, while the friction factor increased between 18% and 25%. In a similar way, Aris et al. [36] studied the effect of SMA delta wings acting as vortex generators for convective cooling, using air as working fluid, and demonstrated the effectiveness of this device on heat transfer enhancement.

Later, Vilarrubí et al. [37], proposed using a SMA wing as an adaptable structure that extends into the flow and modifies the convective heat transfer of a liquid cooling channel. The working principle of the wing was based on the *Two-Way Shape Memory Effect* (TWSME) of trained SMA wings. Through this training, the wing elevates into the flow when a critical temperature is reached, both enhancing the heat transfer and generating a vortex in the fluid to disturb the flow. Contrarily, when the wing is cooled down, it returns to the initial flat shape to reduce the pressure drop in the channel and thus, the pumping power. This work experimentally demonstrated that, the thermally activated wing could provide high temperature uniformity at low pumping power without a custom design. Also, it was observed that the reduction in thermal resistance using trained SMA wings could maintain a surface temperature constant even though the heat flux increases. For a variable heat flux changes from 32.8 to 67 W/cm^2, the presented cooling device was able to maintain the junction temperature within an interval of 7 °C for fixed inlet coolant temperature and flow rate, while the expected temperature difference without the self-adaptive wing was quantified in more than 85 °C.

To further extend our initial paper [37], the present work evaluates the impact of an array of self-adaptive SMA fins on the thermo-hydraulic performance of a mesoscale rectangular channel. In this way, the main objectives of this study are as following:

(a) Design of the mesoscale cooling device with self-adaptive SMA fins, studying numerically the parameters of the self-adaptive cooling system that will ensure an efficient thermal management for mesoscale applications.
(b) Definition of the fabrication and training procedure of the SMA fins to reach the desired behavior of self-adaptation inside a mesoscale cooling system.
(c) Assessment of the impact of the self-adaptive fins in an experimental test bench to evaluate the thermal enhancement with respect to a rectangular plain channel and compare the results with those obtained in the CFD models.

2. Self-adaptive fins working principle

The self-adaptive movement of the fins with temperature is based on the phenomenon of Shape memory effect (SME) in which a material recovers to its original size and shape when heated above a certain characteristic transformation temperature. The shape memory effect has been found in several alloys (SMA) [38] which present the work cycle shown in Fig. 1 when they change crystallographic phase as a function of temperature.

Manufacturing fins from SMA allows the fins to modify their height according to their own temperature in order to adapt the heat extraction capacity. When the SMA temperature is below the starting temperature of the austenite phase transformation (Fig. 1, As), the SMA fins remains in the martensitic phase, maintaining the flat shape without perturbing the coolant flow. However, when SMA is heated above the austenite start temperature (A_s) and towards the austenite finish temperature (A_f), the fins bend upward overcoming the external force applied by a metal sheet coupled with the SMA. The reason behind this movement is the increase in the Young's modulus of the SMA with temperature as it changes from the martensitic to the austenitic phase.

Then, when the cooled base reduces the temperature below the martensitic finish temperature (M_f), a reverse martensitic transformation occurs causing a decrease in the Young's modulus of the SMA. As a consequence, the strain produced by the metal sheet coupled to the SMA increases producing a SMA fins bending back to their flat position.

As a result, the self-adaptive liquid cooling device can generate a time-dependent distribution of thermal resistance adapted to the local requirements of a water-cooled object by using SMA active fins. The local temperature increase promotes the SMA fins change to the austenitic phase, generating a vortex within the flow and enhancing the local heat transfer. Once cooled down, the fin returns to its initial flat shape minimizing the pressure losses and, therefore, the pumping power. Fig. 2 shows the main concept operation for several heat flux distributions.

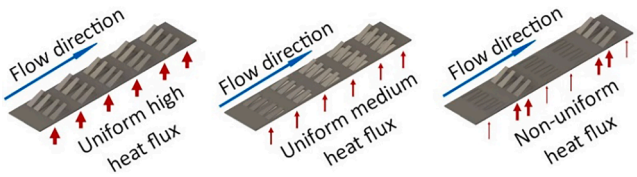

Fig. 2. Working principle of the cooling channel with SMA fins.

3. Mesoscale cooling device design

The impact of self-adaptive fins on the thermo-hydraulic performance of a single channel device is numerically assessed in this section and compared with the performance of a plain channel. It is known that several fin and channel geometric parameters have strong influence on heat sink performance. In this work, fluid flow and heat transfer characteristics of a liquid-cooled channel with different fin shape, channel height and fin distribution are evaluated to find an optimum heat sink configuration.

The fins impact on the thermo-hydraulic performance of the liquid-cooled channel is evaluated in terms of heat transfer enhancement, computed as Nusselt number increment respect a smooth channel (Nu/Nu_0), and pressure drop increment, computed as Fanning friction factor rise respect a plain channel (f/f_0). Nusselt number and Fanning friction factor computations have been defined here below (1),(3). Finally, the thermal performance factor (TPF) is used to account both effects on the performance enhancement of the cooled channel (4).

$$Nu = \frac{hD_h}{\kappa} \tag{1}$$

Where h is the convective heat transfer coefficient ($W/m^2{\cdot}K$), D_h is the hydraulic diameter for non-circular cross section (2) and κ is the conductive heat transfer coefficient ($W/m{\cdot}K$)

$$D_h = \frac{4A}{p} = \frac{2W_{ch}H_{ch}}{(W_{ch} + H_{ch})} \tag{2}$$

$$f = \frac{2\Delta P D_h}{\rho_f L_{ch} v_f^2} \tag{3}$$

Where ΔP is the pressure drop across the fluidic channel, ρ_f is the fluid density, L_{ch} is the channel length and v_f is the fluid velocity.

$$TPF = \frac{\frac{Nu}{Nu_0}}{\left(\frac{f}{f_0}\right)^{\frac{1}{3}}} \tag{4}$$

All geometric parameters of channel and fins are detailed in Fig. 3 and Table 1.

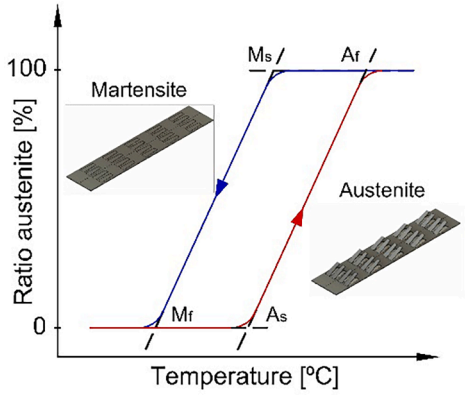

Fig. 1. Ideal work cycle of the SMA fins of martensitic phase transformation. As (f): austenite start (finish) temperature; Ms(f): martensite start (finish) temperature.

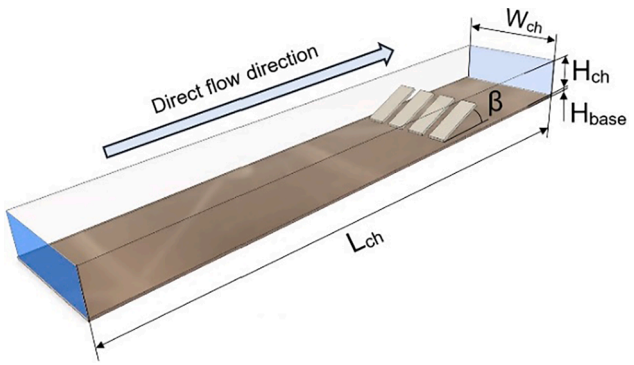

Fig. 3. Schematics of the liquid-cooled channel with one row of SMA fins inside.

Table 1
Main dimensions of the coolant channel and fins.

H_{ch}	$3.5{\cdot}10^{-3}$	m	Channel height
L_{ch}	$5.0{\cdot}10^{-2}$	m	Channel length
W_{ch}	$1.0{\cdot}10^{-2}$	m	Channel width
H_{base}	$2.0{\cdot}10^{-4}$	m	Channel base height
β	23.5	°	Fin inclination resp. channel base
H_{fin}/H_{ch}	0.57	(-)	Fin rise respect channel height

3.1. Boundary conditions and general equations

At the channel inlet, the flow is considered fully developed, with constant flow rate Q = 420 ml/min (Re = 1037), which ensures a maximum chip junction temperature of 85 °C. The inlet coolant temperature is settled to 20 °C and a constant heat flux q''= 30 W/cm^2 is applied at the bottom surface. Flow direction is settled as *direct-flow* when the fluid enters the channel from left to right (Fig. 3) and *counter-flow* when the fluid direction is inversed. In this case, numerical simulations are performed in counter-flow. COMSOL Multiphysics software is used to perform the CFD simulations

The fluid flow is assumed to be laminar, steady, incompressible, and Newtonian, with gravitational effects neglected. Also, the flow is considered hydraulically fully developed and thermally developing, with adiabatic wall at the microchannel cover and no slip boundary condition at walls. The water properties of density (ρ_f), dynamic viscosity (μ_f), specific heat ($C_{p,f}$) and thermal conductivity (κ_f) are calculated for temperature dependence, while the properties of cooper and nitinol are assumed constant due to low changes with temperature (κ_{Cu} = 400 W/m·K, κ_{NiTi} = 18 W/m·K [39]).

The governing equations for the flow are the continuity equation for conservation of mass and the Navier-Stokes equations for conservation of momentum (5), (6) [40].

$$\nabla\cdot(\rho_f \boldsymbol{u}) = 0 \tag{5}$$

$$\rho_f(\boldsymbol{u}\cdot\nabla)\boldsymbol{u} = -\nabla P + \nabla\cdot\mu_f\left[\nabla\boldsymbol{u} + (\nabla\boldsymbol{u})^T\right] \tag{6}$$

The energy equations for liquid (7) and solid (8) are also defined in function of the absolute temperature [41].

$$\nabla\cdot(\rho C_p \boldsymbol{u} T) = \nabla\cdot(\kappa_f \nabla T) \tag{7}$$

$$\kappa_s \nabla^2 T = 0 \tag{8}$$

To ensure the independency of the results from the grid size, a mesh sensitivity analysis has been carried out. The mesh is based on tetrahedral elements and 2 fluid boundary layers and has been found that, with a mesh bigger than $1{\cdot}10^6$ elements, the relative error compared with the finest grid size is lower than 1%, which is considered acceptable. In this case, the selected mesh is based on 1,046,798 elements, with relative errors in ΔP and T_{chip} lower than 0.50 % and 0.56 %, respectively.

3.2. Fin shape impact

Two different fin geometries (rectangular and trapezoidal) are proposed to evaluate fin shape impact on the thermo-hydraulic performance of the cooling channel (Fig. 4). Results obtained within each fin geometry are listed in Table 2.

Results from Table 2 show that rectangular fins present the highest cooling capacity, as they are able to reach lower convective thermal resistances and enhance heat transfer by 16 % compared with a plain channel. Nevertheless, large pressure drop increment leads to a reduced thermal performance factor (TPF) compared with the others assessed geometries. Although maximum reduction in pumping power is always desired, it is important to notice that the increment in pressure drop due to the addition of the fins inside the channel is not a key parameter in our device due to the self-adaptation concept. In this case, the pressure drop

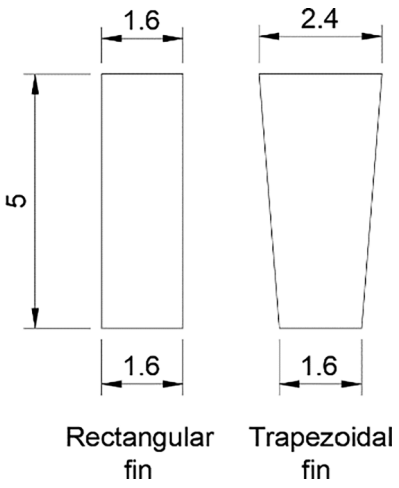

Fig. 4. Different fin shapes assessed (units in mm).

Table 2
Cooling channel performance with different fin shape.

Fins shape	$T_{chip,\ av}$ [ºC]	$T_{f,\ OUT}$ [ºC]	Nu/Nu_0 [-]	f/f_0 [-]	TPF [-]
Plain channel	75.0	28.7	–	–	–
Rectangular	67.3	26.4	1.16	1.61	0.99
Trapezoidal	68.6	26.3	1.13	2.24	0.78

increment will be reached only when high heat extraction is demanded, otherwise it will be significantly reduced as the fins will remain in a flat position.

CFD simulations show that in the upper part of the channel, between the fin and the top wall, the fluid does not tend to mix (Fig. 5). Therefore, the next step will be to analyze the effect of a new parameter, the ratio between channel and fin heights or the occupancy ratio (H_{fin} / H_{ch}).

3.3. Channel height impact

As seen in the previous section, low mixing is viewed in the upper part of the channel and so, with the aim of increasing heat transfer due to the addition of the fins, the channel height is reduced up to 2.5 mm to increase the ratio between fin rise and channel height from 0.57 to 0.8. Fluid velocity is unchanged when decreasing channel height. Results evaluating the impact of rectangular and trapezoidal fins on the cooling performance of 2 different channels, with height of 2.5 mm and 3.5 mm, respectively, are detailed in Table 3.

Table 3 shows that by increasing the height ratio, there is a gain in heat transfer. This is reflected in terms of the reduction of T_{chip}, and in increased Nu/Nu_0.

On the other hand, this reduction in channel height has a negative effect in terms of pressure, reaching a duplication of f/f_0 in the case of trapezoidal fins. As stated before, the pumping power increment is not considered a major key point on the design of the optimal self-adaptive heat sink configuration due to the lack of permanency. In this way, the enhancement of the channel cooling capacity due to the height reduction is considered more beneficial than the pressure drop increment.

Assessing both results from previous and present section, it is foreseen those rectangular fins with a ratio fin to channel height equal to 0.80 offers good performance. An enhancement in heat transfer similar to trapezoidal fins with lower pressure drop is achieved, what results to an improved and optimized liquid-cooled heat sink with rectangular self-adaptive fins inside.

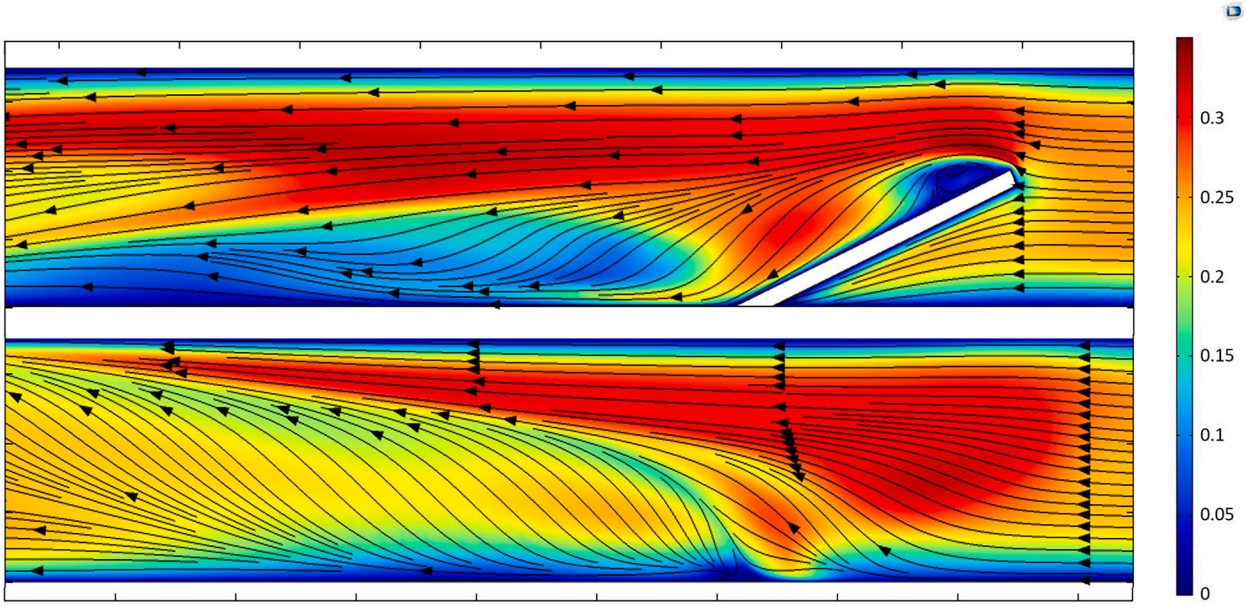

Fig. 5. Velocity longitudinal planes a) at middle of fin b) between fins.

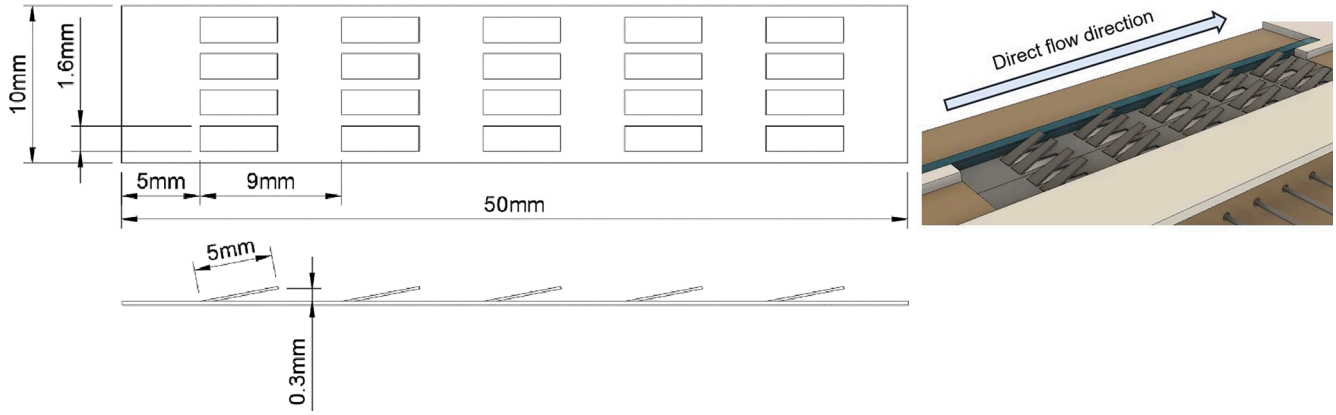

Fig. 6. Schematic of the liquid-cooled channel with the new fin distribution considered (left side) and isometric image of the SMA fins sample in austenitic phase (right side).

Table 3
Channel height and fin shape impact on the thermo-hydraulic performance of a cooling channel.

Fins shape	H_{ch} [mm]	$T_{chip,av}$ [ºC]	$T_{f,\ OUT}$ [ºC]	Nu/Nu0 [-]	f/f0 [-]	TPF [-]
Plain channel	2.5	75.0	28.7	–	–	–
	3.5	75.0	28.7	–	–	–
Rectangular	2.5	62.6	28.6	1.29	2.86	0.91
	3.5	67.3	26.4	1.16	1.61	0.99
Trapezoidal	2.5	62.1	28.6	1.31	4.48	0.80
	3.5	68.6	26.3	1.13	2.24	0.78

3.4. Fin distribution impact

Up to now, the impact of the fins on the cooling performance of a liquid cooled channel has been evaluated considering a unique row of self-adaptive fins, as detailed in Fig. 3. In this section, a different distribution of fins along the channel, based on 5 rows of 4 fins in each, is studied. Both previous assessed parameters – fin shape and channel height- can't be settled due to experimental limitations. The average lift of the fins is 0.3 mm, which means that the ratio H_{fin} / H_{ch} = 0.8 cannot be maintained if numerical results and experimental results have to be compared. For this reason, the conditions have been modified in this section by setting H_{ch} = 1 mm and H_{fin} = 0.3 mm. Results obtained are detailed in Table 4.

In the previous simulations, the material of the fins was considered copper because we unknown exactly which NiTinol be used. In this section, to ensure good comparison with experimental results, the material of the fins and channel base is considered NiTinol (nickel-titanium composed).

Obtained results show that the cooling capacity of a liquid-cooled channel with NiTinol fins is increased by 31% (Table 4) compared with a plain channel. Taking into consideration the thermal performance factor and the Nusselt number as figures of merit, this

Table 4
Comparison of thermo-hydraulic performance of liquid-cooled channel without fins and with SMA and Cu fins.

Design	$T_{chip,av}$ [ºC]	$T_{f,OUT}$ [ºC]	Nu/Nu0 [-]	f/f0 [-]	TPF [-]
Plain channel	53.9	28.50	–	–	–
SMA Fins device	45.7	28.53	1.31	3.05	0.904
Cu Fins device	42.2	28.45	1.53	3.05	1.057

numerically evaluated design is an interesting configuration that offers theoretical advantages in water-cooled applications. In addition, the use of fixed copper fins is considered, to compare the performance of SMA self-adaptive fins over fixed fins acting as traditional vortex generators. Due to the highest thermal conductivity of cooper, the heat conduction is increased from the fin to the base, resulting in a 53% increase in heat extraction over the plain channel. As the resulting TPF is higher than one, the use of fixed copper fins implies an energetic improvement with respect to the empty channel when applying steady state heat load scenarios.

However, the thermal demand under operating conditions of electronics vary spatially and temporally, leading to transient high load scenarios. Consequently, decreasing the SMA fins height in the background load intervals to reduce the pressure drop at 1/3 (Table 4) provides an important pumping power saving. Since the fins are deformed according to their own temperature, a self-regulation of the heat extraction occurs depending on the thermal needs allowing to minimize the pumping consumption without external control. The energy savings provided by self-adaptive fins increase with the time contribution of the background duty cycle and potentially exceed the savings achieved with fixed fins made of higher thermal conductive material such as copper.

4. Experimental setup and tests

4.1. Experimental test bench

The impact of self-adaptive fins on the thermo-hydraulic performance of a liquid cooling device at mesoscale is experimentally assessed in this section. Fig. 7 illustrates the schematic design of the experimental apparatus employed in this work.

The experimental setup is based on two separated hydraulic circuits (Fig. 7). In the first one, the water is stored in a thermostatic bath (PolyScience PD07R20-20-A12E) which is connected to the heat exchanger responsible for heating or cooling the water of the second circuit. This second circuit is composed of a 1 μm filter (Shelco MPX) connected to a flowmeter (Bronkhorst mini cori-flow M15, 600 ml/min FS, ±0.2 % of rate) and then to a micro-diaphragm liquid pump (KNF NF series) that reaches a maximum flow rate of 300 ml/min and a maximum pressure of 1 bar. A diaphragm pulsation damper (KNF FPD06/1.06-Z), placed after the pump, is responsible for flow stabilization before it enters the heat exchanger. Then, the test module is hydraulically connected to the heat exchanger and finally the water returns to the filter.

The test module is heated with a ceramic heater (Watlow Ultramic 600) that can give up to 155 W/cm^2 and is electrically connected to a programmable power source (PSI9200-04 T) that can be controlled by LabVIEW software.

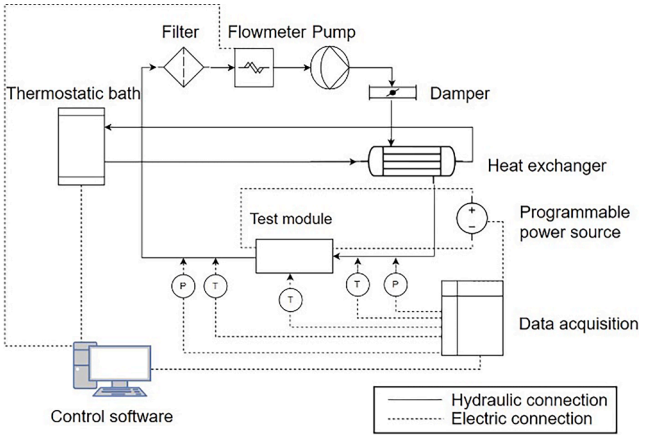

Fig. 7. Test module setup scheme.

Type-T thermocouples (Omega – TJC100, ±0.1 °C) are used to measure the water temperature at the inlet and outlet of the fluid channel and the temperature distribution in the copper layer along the flow path at the centreline of the channel base. Also, low range industrial pressure sensors (RS PRO - IPSL Series, (±83.5 Pa) are used to measure the water pressure at the inlet and outlet of the channel.

Propagation of experimental errors in the different calculations is computed as detailed in *(9)*, where the absolute error is assessed as a function of an associated error (Δx, Δy, Δz) for the experimental parameters (x, y, z).

$$f = \frac{(x+\Delta x)(y+\Delta y)}{(z+\Delta z)} = \left(\frac{xy}{z}\right) \pm \left(\frac{xy}{z}\right)\sqrt{\left(\frac{\Delta x}{x}\right)^2 + \left(\frac{\Delta y}{y}\right)^2 + \left(\frac{\Delta z}{z}\right)^2} \quad (9)$$

4.2. Test module

The test module shown in Fig. 8 is composed of a PET-G coolant manifold, a polycarbonate part that forms the cooling channel and a thermoplastic base with a gap where a copper layer and a ceramic heater are assembled. Both the base and the copper layer are drilled to allow the insertion of thermocouples.

The main geometrical values are detailed in Fig. 8.b, which shows the 3D design in top view and cross-section A of the cooling device. The coolant fluid enters to the manifold from a polyurethane tube and descends vertically to the cooling channel (Fig. 8.a) and returns to the pipe circuit through the outlet connection. When there is no sample, a ceramic heater provides a homogeneous heat flux that is transmitted through a cooper plate that contains 13 thermocouples which operates as the bottom channel wall. The fins sample tested is bonded to the copper plate through a thermal interface material (TIM, $\lambda_{TIM} = 8.9$ W/m·K). Channel walls are made from polycarbonate parts with thickness of 10 mm in the back camera side and 1.5 mm in the front camera side.

4.3. Self-adaptive fins sample

Among the different materials that present the intrinsic property of *One Way Shape Memory Effect* (OWSME), the Ni-Ti alloy results suitable as a self-adaptive component in the cooling system due to its favorable properties related to corrosion, ductility and recoverable deformation [42]. However, the cyclic movement of the self-adaptive fins requires either the application of an additional training or an external force to exhibit a shape recovery effect upon cooling.

The training method known as *Two-Way Shape Memory Effect* (TWSME) is an interesting technique to achieve the cyclic movement because it offers many advantages in the simplicity of the sample design [43]. However, this method is not deployed in the fins sample tested in this study since TWSME method presents several disadvantages such as low stroke between phases, higher complexity in its fabrication due to the required "training" and instability of the displacement over its lifetime [44]. As a result, the fin sample tested is made of an SMA with a final austenitic temperature of 85 °C whose movement is based on one-way shape memory effect acting coupled with an external stress. This bimorph fins concept employs an external force to recover the flat fins position when the temperature decreases. The fins sample has been developed and manufactured by *Memetis* GmbH (Fig. 9) that is composed by SMA sheet coupled with another metallic sheet.

4.4. Fatigue life

The effect of the working cycles has been investigated on the bimorph SMA/metallic fins to consider the degradation of the shape memory property in our application. The expected fatigue life which typical shape memory components must withstand in service depends on the application for which the product is designed.

However, the typical number of duty cycles to be expected for a

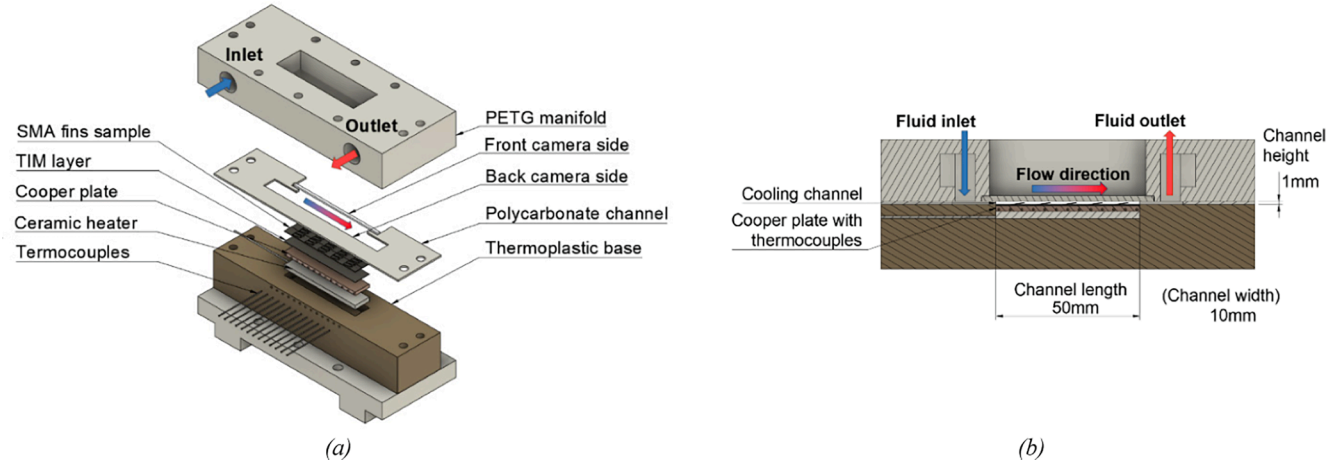

Fig. 8. Exploded view of the cooling test module (a) and cross-section of the cooling device with main geometrical values (b).

Fig. 9. Bimorph metallic/SMA sample.

thermo-hydraulic valve using OWSME is 10,000 cycles [45]. Due to the similarity in functionality and working conditions with respect to the self-adaptive fins, a thermo-hydraulic value of expected duty cycles is taken as a reference for the number of thermal cycles to be tested for validating the functional fatigue of the self-adaptive fins.

The results of analyzing 10,000 thermomechanical cycles show that the SMA suffers functional degradation causing a decrease in displacement as the cycles increase. In particular, there is a rather strong decay of maximum fins height in the early stage of working and the degradation rate decreases in the latter stage. In fact, the height loss after 6,000 cycles is almost negligible, so the height value stabilizes at 55,6% of its initial value allowing the SMA fins to remain in service.

4.5. Boundary conditions

A fixed flow rate of 285 ml/min is applied in all the tests (Reynolds number of 862) and the channel height is reduced to 1 mm to maintain the ratio of 0.8 between experimental fin rise and channel height. Water inlet temperature is settled at 62 °C to allow the fins to modify their height in function of the heat flux scenario while avoiding water boiling.

Two different time dependent heat load scenarios, both remaining enough time in each interval to reach steady state temperatures, are defined:

- q''_1: based on a step signal increasing from 3 W/cm^2 to 11 W/cm^2 with a step duration of 120 s for each of the 5 power intervals.
- q''_2: based on a pulse signal of 9 W/cm^2 and background of 3 W/cm^2 with a step duration of 300 s.

5. Experimental results

5.1. Base temperature uniformity along the cooled device

5.1.1. Direct-flow direction

The effect of power density on the maximum wall temperature difference is assessed in both a plain channel (Fig. 10) and a channel with SMA fins (Fig. 11) when q''_1 is applied and flow direction along the channel path corresponds to *direct-flow* as shown in Fig. 6.

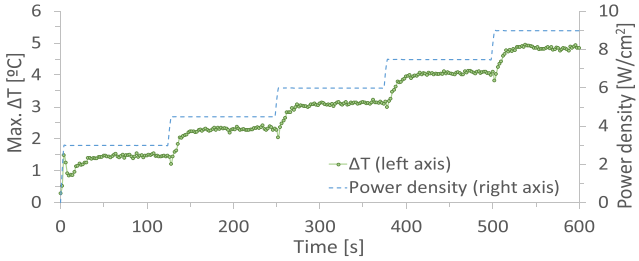

Fig. 10. Experimental maximum temperature difference along a plain channel when applying q''_1 (±0.14 °C, ±713 mW/cm^2).

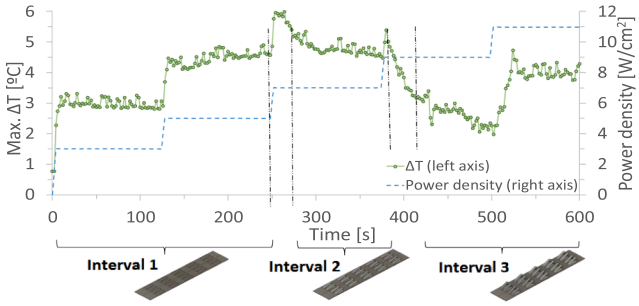

Fig. 11. Experimental maximum temperature difference along the channel with SMA fins when applying q''_1 (±0.14 °C, ±713 mW/cm^2).

Analogous thermo-hydraulic behavior in temperature gradient is observed from 0 to 5 W/cm^2 in both cases, since the SMA fins remain in flat position (Interval 1 in Fig. 11). Nevertheless, the SMA fins start to rise when the power density increases to 7 W/cm^2 (Fig. 11, t = 240 s) and after a transient period of 50 s, the fins reach an elevation of 37% of the channel height (Fig. 11, t = 290 s). Fig. 12 shows an image recording of the fins position in function of the time intervals indicated in Fig. 11. During interval 2, the thermal gradient keeps almost constant until the next power step, that makes the fins increase its height again (Fig. 11, t = 360 s) during 60 s until the fins reach the maximum height of 74 % of channel height (Fig. 11, t = 420 s). However, the thermal gradient in interval 3 continues to decrease as a consequence of the thermal inertia of the system to reach the equilibrium temperature by the enhanced cooling capacity by the fins. As a result, the thermal gradient at 9 W/cm^2 is lower than the one produced at 3 W/cm^2, when the fins are not raised. Finally, thermal gradient increases in the last power stage since the

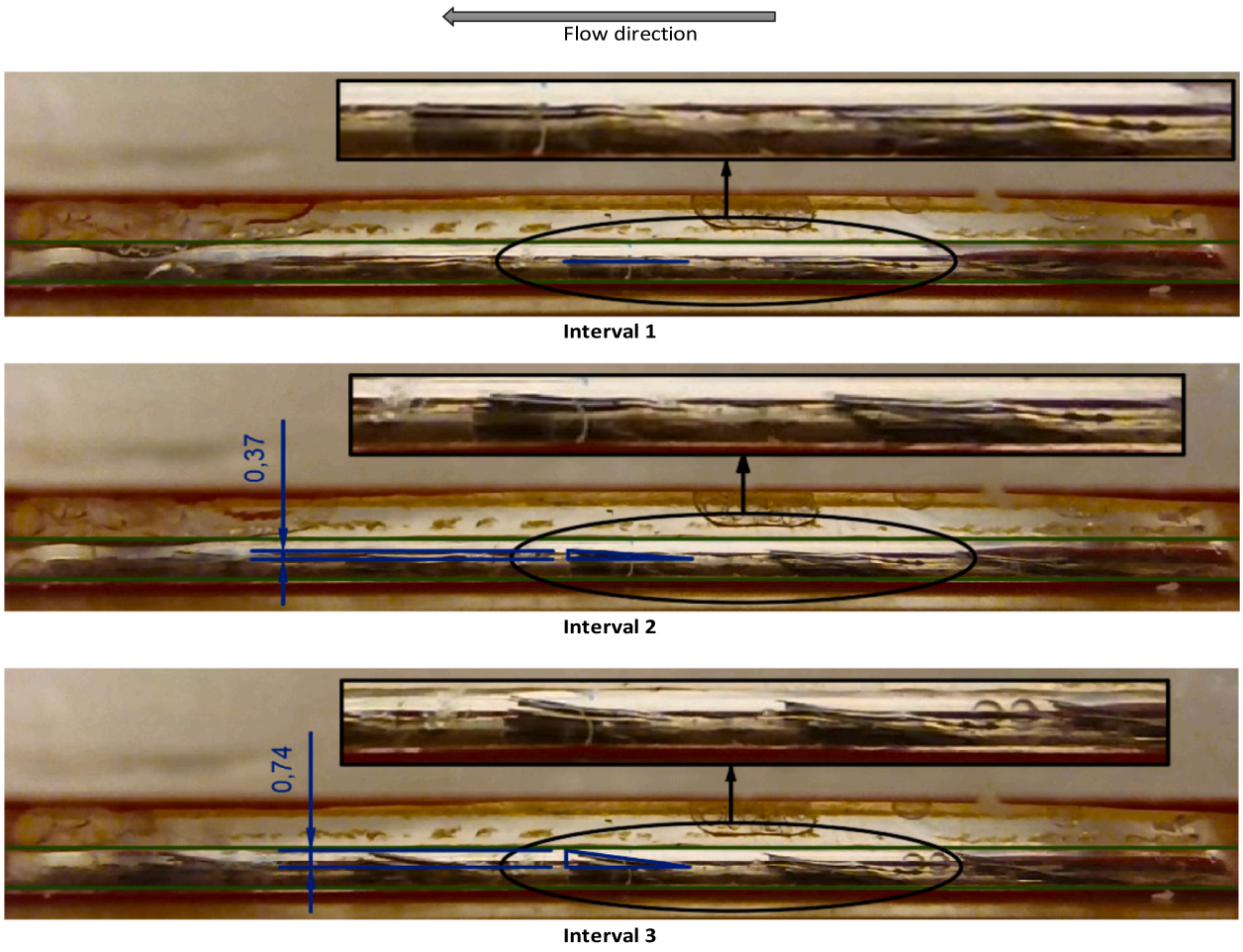

Fig. 12. Images of the cooling channel with SMA fins regarding the different time periods detailed in Fig. 11.

thermal resistance is maintained because the SMA fins are already in the highest position.

Fig. 13 shows the maximum temperature difference obtained at channel wall when applying q''_2 in order to assess both steady and transient states. Here, the SMA fins rise up when the power density increases from 3 W/cm^2 to 9 W/cm^2 (Fig. 13, t = 300 s) causing a progressive temperature gradient decrement during 200 s, which stabilizes at interval 2, with fins raised 49% of the channel height (Fig. 13, t = 500 s).

In this case it is observed the transient effect of the thermal gradient decrease due to the fins rising. Specifically, when 9 W/cm^2 are applied, the temperature gradient decreases from 5.4 ℃ to 2.0 ℃ depending on whether the channel is plain or contains the fins in raised position. Thus, it is experimentally demonstrated that the self-adaptive fins are able to improve the channel temperature uniformity by 63% through acting as flow disturbing elements able to break the flow boundary layer and enhance the convection heat transfer.

5.1.2. *Counter-flow direction*

In this section, the impact of the fins on the cooling channel performance is evaluated with the coolant flowing in the opposite direction to the previous one. Thus, Fig. 14 shows the channel base temperature gradient evolution when q''_1 is applied.

Initially, the fins are in a horizontal position (martensitic phase) during the entire interval 1. Then, when the power density is increased to 6 W/cm^2, the fins start to rise (Fig. 14, t = 240 s), considerably reducing the thermal gradient increase that would be expected in a plain channel. The fins continue to rise for 50 s (Fig. 14, t = 290 s) when 27%

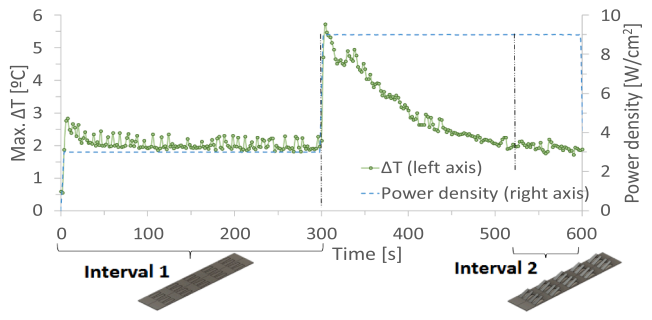

Fig. 13. Experimental maximum temperature difference along the channel with SMA fins when applying q''_2 (±0.14 °C, ±713 mW/cm^2).

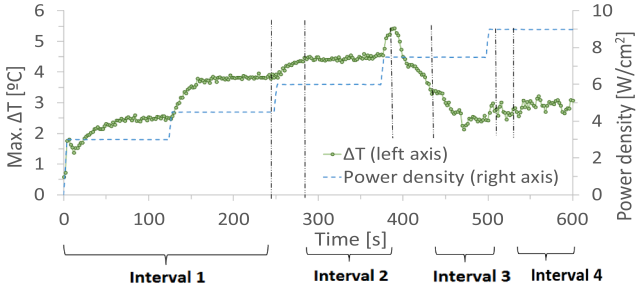

Fig. 14. Evolution of maximum temperature difference along channel base with the cooling device with SMA fins when applying q''_1 (±0.14 °C, ±713 mW/cm^2).

of the channel height is reached by the fins.

Then, by increasing the power density to 7.5 W/cm^2 there is another increase of the fins height (Fig. 14, from t = 380 s to t = 430 s), where the thermal heat transfer is improved, resulting in a thermal gradient lower than that at 3 W/cm^2 when the fins were in flat position. Finally, when the power density is increased to 9 W/cm^2, the thermal gradient stabilizes slightly above the value of the previous interval.

All of the preceding tests show that the fins sample is able to modify the thermal resistance allowing the maximum temperature gradient of the surface to remain almost constant even as the heat flux increases. For heat flux changes from 2 to 9 W/cm^2, the cooling device can maintain a temperature gradient of 2 °C for fixed inlet coolant temperature and flow rate. This value is remarkably smaller than the 7 °C of thermal gradient in the absence of the fins sample.

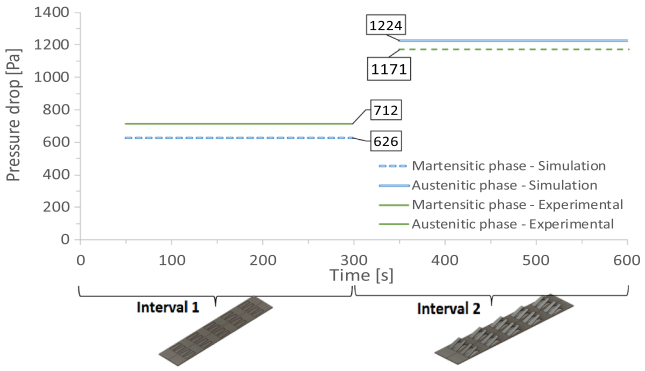

Fig. 16. Average pressure drop along the channel according to simulation and experimental results for inlet fluid temperatures of 20 °C and 80 °C to define the martensite and austenite phases, respectively (±83,5 Pa).

5.2. Heat transfer enhancement

The effect of the self-adaptive SMA fins on the convective heat transfer coefficient of the cooled channel is experimentally evaluated in this section with the coolant flowing in counter flow direction. First, the total thermal resistance (conduction + convection) is experimentally evaluated in both the channel with flat fins and with elevated fins. The convective heat transfer coefficient is calculated as the inverse of the difference between the total experimental thermal resistance and the thermal conduction resistance of the sample assembly, according to whether the phase of the SMA fins is martensitic ($5.32 \cdot 10^{-4}$ m^2·K/W) or austenitic ($3.64 \cdot 10^{-4}$ m^2·K/W). Fig. 15 graphs the convective heat transfer coefficient of the device with both SMA phases as a function of time when heat load scenario q''_2 is applied.

The solid line in Fig. 15 shows the instantaneous values of convective heat transfer coefficient on the channel with SMA fins, while dashed lines represents mean convective value during each crystallographic phase.

When a low heat flux (interval 1) is applied, the SMA fins remain in a flat position resulting in the same convection coefficient than within a plain channel without fins. However, when high heat flux is applied (interval 2) the SMA fins rise up to 30 % of the channel height resulting in a heat transfer enhancement about 50 % higher than the one of the channel with flat fins. This experimental result is higher than the 31% value obtained from the numerical simulations presented in Section 3.4 for the SMA fins, but lower than the 53% value obtained for the copper fins. The reason can be attributed to the additional thermal conduction provided by the experimental SMA fins due to the additional conduction through the metallic sheet used to apply the external force to recover the flat position of the fins.

5.3. Pressure drop and thermal performance factor

The added value of the self-adaptive fins depends strongly on the savings in pumping power achieved when the thermal demand decreases by decreasing their height and, therefore, the pressure drop. In this section, the tests to evaluate the pressure drop of the fluid passing through the channel with the fins raised and with the fins flat are

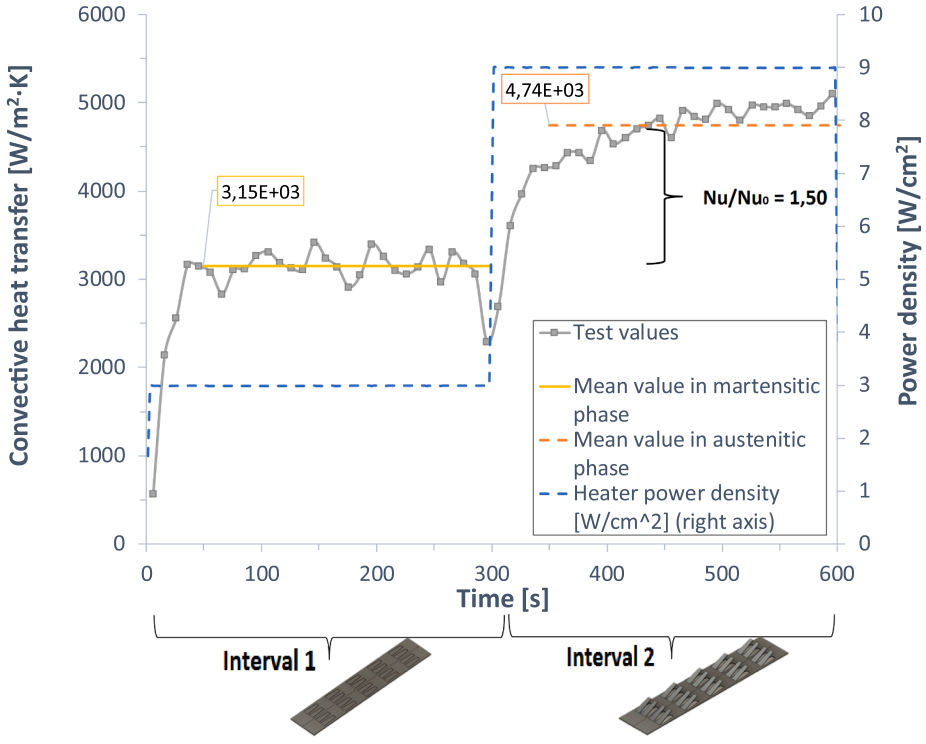

Fig. 15. Experimental convective heat transfer coefficient for channel with SMA fins in martensitic and austenitic phases, when applying heat load scenario q''_2 (±376 W/m^{2}K, ±713 mW/cm^2).

presented (Fig. 16). To achieve the same temperature in all fins and to maximise the equal height between them at 0.3 mm, a constant flow rate is defined as a boundary condition at 20 °C and then at 80 °C to define the martensite phase (flat fins) and austenite phase (raised fins), respectively. These same boundary conditions are defined in the CFD simulations for the validation of the numerical model used in Section 3.4.

The results of the pressure drop show a difference between the experimental values and the CFD simulation of 4.5% when the fins are raised and 12% when the fins are flat. It should be noted that the CFD simulation considers the fins in a perfectly flat position while experimentally the fins show some roughness due to the deformation of the materials that compose them. Considering also the uncertainty of the sensors of ±83.5 Pa, the match between the two models validates the pressure drop of the CFD model reported in Section 3.4.

Since the pressure drop tests have been carried out at different inlet fluid temperature and once the results of the numerical model have been validated, the experimental TPF is calculated using the experimental Nu/Nu_0 of 1.50 and the f/f_0 factor of 3.05 from the simulated model. As a result, a TPF value of 1.034 is obtained, while the simulated values are 0.904 for SMA fins and 1.057 for copper ones. The experimental TPF is near to the corresponding one for copper fins because of the close heat transfer gain as the experimental device has an additional metallic sheet which enhances the heat conduction with respect to the SMA material. Nevertheless, TPF is not considered a key parameter on the design of the self-adaptive fins, as it will depend on the position of the fins and will vary in function of the heat load applied.

6. Conclusions

The proposed concept of SMA self-adaptive fins inside a liquid cooling channel has been numerically and experimentally demonstrated in this work.

First, the optimum configuration of different fins geometric parameters to maximize its impact on the thermo-hydraulic performance of a liquid-cooled device has been numerically assessed. In this way, it has been seen that although, trapezoidal fins achieve larger heat transfer enhancement, rectangular fins offer a good balance between heat transfer enhancement and pressure drop increment. Also, the impact of the ratio fin to channel height has been numerically evaluated, resulting in both higher heat transfer enhancement and pressure drop when the height of the channel was reduced.

After defining the optimum numerical configuration of the liquid cooled channel with SMA self-adaptive fins and describing the set of testing conditions, a series of experimental tests have been carried out at fixed flow rate while applying different time dependent and uniform heat load scenarios.

It has been observed that the maximum base temperature when using self- adaptive fins is reached at 30 % of the channel flow path rather than at the end of the channel, where is expected to occur in a plain channel. Additionally, self-adaptive fins improve the temperature uniformity by 63.1 % with respect to a plain channel. This significant reduction in the thermal gradient along the channel when the fins are raised, confirms the heat transfer enhancement due to the fins acting as flow disturbing elements along the entire flow.

It has been seen that the reduction in thermal resistance when using bimorph metal/SMA fins allows the maximum temperature gradient of the surface to remain almost constant even though when the heat flux increases. For fixed inlet coolant temperature and flow rate, the cooling device was able to maintain the temperature within a temperature gradient of 2 °C under heat flux variations from 2 to 9 W/cm^2, compared to an increase of more than 7° C in a channel without fins.

The CFD model showed an improved cooling capacity of the liquid-cooled channel with fins raised 30% of the channel height. SMA fins improved the heat transfer by 31% and copper fins by 53% compared with a plain channel. However, experimental tests shown that raised SMA fins could improve heat transfer enhancement by 50 % compared with the fins in a flat position. The reason behind can be attributed to the additional thermal conduction provided by the experimental SMA fins due to the additional conduction through the metallic sheet used to apply the external force to recover the flat fins position.

The results of the pressure drop show a difference between the experimental values and the CFD simulation of 4.5% when the fins are raised and 12% when the fins are flat. Considering the additional roughness of the experimental fins and the uncertainty of the sensors, the experimental results validate the pressure drop and TPF of the CFD model, that showed an increment of more than 300% in pressure drop due to raised fins. The self-adaptive behaviour of the fins enables the raised shape only during high thermal load scenarios, thus reducing the time with additional pressure drop inside the cooling channel. Consequently, the use of self-adaptive fins offers savings in pumping power as the pressure drop is reduced to 1/3 during low thermal load scenarios compared to a system with static fins. Therefore, energy savings are maximized by using the auto-adaptive system in those applications where the time contribution of the background duty cycle contribute significantly to the overall operating period.

Declaration of Competing Interest

The authors declare that they have no known competing financial interests or personal relationships that could have appeared to influence the work reported in this paper.

Acknowledgement

The research leading to these results has been performed within the project Indústria del Coneixement 2018, PROD-00071 "*Experimental demonstration and commercial viability of an energy efficient universal cooling scheme*". It has been co-financed by the European Union through the European Regional Development Fund (FEDER) and has the support of the *Secretaria d'Universitats i Recerca* from Departament d'Empresa i Coneixement of the Generalitat de Catalunya.

References

[1] M. Graef, B. Huizing, R. Mahnkopf, H. Ishiuchi, Y. Hayashi, N. Ikumi, H. Miyakawa, S. Choi, J. Hoon Choi, S. Pam, W. Tsai, P. Gargini, T. Kingscott, L. Wilson, International technology roadmap for semiconductors 2 (2015).

[2] D.B. Tuckerman, R.F.W. Pease, High-performance heat sinking for VLSI, IEEE Electron Device Lett. 2 (5) (1981) 126–129, https://doi.org/10.1109/EDL.1981.25367.

[3] C.S. Sharma, S. Zimmermann, M.K. Tiwari, B. Michel, D. Poulikakos, Optimal thermal operation of liquid-cooled electronic chips, Int. J. Heat Mass Transf. 55 (7-8) (2012) 1957–1969, https://doi.org/10.1016/j.ijheatmasstransfer.2011.11.052.

[4] B. Sinharoy, R. Kalla, W.J. Starke, H.Q. Le, R. Cargnoni, J.A. Van Norstrand, B. J. Ronchetti, J. Stuecheli, J. Leenstra, G.L. Guthrie, D.Q. Nguyen, B. Blaner, C. F. Marino, E. Retter, P. Williams, IBM POWER7 multicore server processor, IBM J. Res. Dev. 55 (3) (2011) 1:1–1:29, https://doi.org/10.1147/JRD.2011.2127330.

[5] D. Kearney, T. Hilt, P. Pham, A liquid cooling solution for temperature redistribution in 3D IC architectures, Microelectronics J. 43 (9) (2012) 602–610, https://doi.org/10.1016/j.mejo.2011.03.012.

[6] S.G. Kandlikar, Review and Projections of Integrated Cooling Systems for Three-Dimensional Integrated Circuits, J. Electron. Packag. 136 (2014), https://doi.org/10.1115/1.4027175.

[7] T. Brunschwiler, H. Rothuizen, S. Paredes, B. Michel, E. Colgan, P. Bezama, Hotspot-adapted Cold Plates to Maximize System Efficiency, in: 15th Int. Work, Therm. Investig. ICs Syst. (2009) 150–156.

[8] A.M. Waddell, J. Punch, J. Stafford, N. Jeffers, The characterization of a low-profile channel–confined jet for targeted hot-spot cooling in microfluidic applications, Int. J. Heat Mass Transf. 101 (2016) 620–628, https://doi.org/10.1016/j.ijheatmasstransfer.2016.04.108.

[9] P.-S. Lee, S. V Garimella, Hot-Spot Thermal Management With Flow Modulation in a Microchannel Heat Sink, ASME Int. Mech. Eng. Congr. Expo. (2005) 643–647, https://doi.org/10.1115/imece2005-79562.

[10] Y.J. Lee, P.S. Lee, S.K. Chou, Hotspot mitigating with obliquely finned microchannel heat sink-an experimental study, IEEE Trans. Components, Packag. Manuf. Technol. 3 (8) (2013) 1332–1341, https://doi.org/10.1109/TCPMT.2013.2244164.

[11] S. Lu, K. Vafai, A comparative analysis of innovative microchannel heat sinks for electronic cooling, Int. Commun. Heat Mass Transf. 76 (2016) 271–284, https://doi.org/10.1016/j.icheatmasstransfer.2016.04.024.
[12] G. Hetsroni, A. Mosyak, Z. Segal, G. Ziskind, A uniform temperature heat sink for cooling of electronic devices, Int. J. Heat Mass Transf. 45 (16) (2002) 3275–3286, https://doi.org/10.1016/S0017-9310(02)00048-0.
[13] P.R. Parida, A. Sridhar, A. Vega, M.D. Schultz, M. Gaynes, O. Ozsun, G. McVicker, T. Brunschwiler, A. Buyuktosunoglu, T. Chainer, Thermal model for embedded two-phase liquid cooled microprocessor, in: Proc. 16th Intersoc. Conf. Therm. Thermomechanical Phenom. Electron. Syst. ITherm 2017, Institute of Electrical and Electronics Engineers Inc., (2017) 441–449, doi: 10.1109/ITHERM.2017.7992508.
[14] C.S. Sharma, M.K. Tiwari, B. Michel, D. Poulikakos, Thermofluidics and energetics of a manifold microchannel heat sink for electronics with recovered hot water as working fluid, Int. J. Heat Mass Transf. 58 (1-2) (2013) 135–151, https://doi.org/10.1016/j.ijheatmasstransfer.2012.11.012.
[15] G. Laguna, M. Vilarrubí, M. Ibañez, Y. Betancourt, J. Illa, H. Azarkish, A. Amnache, L.M. Collin, P. Coudrain, L. Fréchette, J. Barrau, Numerical parametric study of a hotspot-targeted microfluidic cooling array for microelectronics, Appl. Therm. Eng. 144 (2018) 71–80, https://doi.org/10.1016/j.applthermaleng.2018.08.030.
[16] T. Brunschwiler, H. Rothuizen, M. Fabbri, U. Kloter, B. Michel, R.J. Bezama, G. Natarajan, Direct liquid jet-impingement cooling with micronsized nozzle array and distributed return architecture, in, Thermomechanical Phenom. Electron. Syst. -Proceedings Intersoc. Conf. (2006) 196–203, https://doi.org/10.1109/ITHERM.2006.1645343.
[17] S.G. Kandlikar, A.V. Bapat, Evaluation of jet impingement, spray and microchannel chip cooling options for high heat flux removal, Heat Transf. Eng. 28 (11) (2007) 911–923, https://doi.org/10.1080/01457630701421703.
[18] J. Barrau, D. Chemisana, J. Rosell, L. Tadrist, M. Ibañez, An experimental study of a new hybrid jet impingement/micro-channel cooling scheme, Appl. Therm. Eng. 30 (14-15) (2010) 2058–2066.
[19] S. Riera, J. Barrau, M. Omri, L.G. Frechette, J.I. Rosell, Stepwise varying width microchannel cooling device for uniform wall temperature: Experimental and numerical study, Appl. Therm. Eng. 78 (2015) 30–38, https://doi.org/10.1016/j.applthermaleng.2014.12.012.
[20] M. Vilarrubí, S. Riera, M. Ibañez, M. Omri, G. Laguna, L.G.L.G. Fréchette, J. Barrau, Experimental and numerical study of micro-pin-fin heat sinks with variable density for increased temperature uniformity, Int. J. Therm. Sci. 132 (2018) 424–434, https://doi.org/10.1016/j.ijthermalsci.2018.06.019.
[21] C.S. Sharma, M.K. Tiwari, S. Zimmermann, T. Brunschwiler, G. Schlottig, B. Michel, D. Poulikakos, Energy efficient hotspot-targeted embedded liquid cooling of electronics, Appl. Energy. 138 (2015) 414–422, https://doi.org/10.1016/j.apenergy.2014.10.068.
[22] C.S. Sharma, G. Schlottig, T. Brunschwiler, M.K. Tiwari, B. Michel, D. Poulikakos, A novel method of energy efficient hotspot-targeted embedded liquid cooling for electronics: An experimental study, Int. J. Heat Mass Transf. 88 (2015) 684–694, https://doi.org/10.1016/j.ijheatmasstransfer.2015.04.047.
[23] M.E. Steinke, S.G. Kandlikar, Single-Phase Heat Transfer Enhancement Techniques in Microchannel and Minichannel Flows, in: ASME 2nd Int. Conf. Microchannels Minichannels, (2004) 141–148, doi: 10.1115/ICMM2004-2328.
[24] N.A.C. Sidik, M.N.A.W. Muhamad, W.M.A.A. Japar, Z.A. Rasid, An overview of passive techniques for heat transfer augmentation in microchannel heat sink, Int. Commun. Heat Mass Transf. 88 (2017) 74–83, https://doi.org/10.1016/j.icheatmasstransfer.2017.08.009.
[25] C. Liu, J.-T. Teng, J.-C. Chu, Y.-L. Chiu, S. Huang, S. Jin, T. Dang, R. Greif, H.-H. Pan, Experimental investigations on liquid flow and heat transfer in rectangular microchannel with longitudinal vortex generators, Int. J. Heat Mass Transf. 54 (13-14) (2011) 3069–3080, https://doi.org/10.1016/j.ijheatmasstransfer.2011.02.030.
[26] A. Datta, D. Sanyal, A.K. Das, Numerical investigation of heat transfer in microchannel using inclined longitudinal vortex generator, Appl. Therm. Eng. 108 (2016) 1008–1019, https://doi.org/10.1016/j.applthermaleng.2016.07.165.
[27] G. Wang, D. Niu, F. Xie, Y. Wang, X. Zhao, G. Ding, Experimental and numerical investigation of a microchannel heat sink (MCHS) with micro-scale ribs and grooves for chip cooling, Appl. Therm. Eng. 85 (2015) 61–70, https://doi.org/10.1016/j.applthermaleng.2015.04.009.
[28] A. Ebrahimi, B. Naranjani, S. Milani, F. Dadras Javan, Laminar convective heat transfer of shear-thinning liquids in rectangular channels with longitudinal vortex generators, Chem. Eng. Sci. 173 (2017) 264–274, https://doi.org/10.1016/j.ces.2017.07.044.
[29] L.H. Tang, W.X. Chu, N. Ahmed, M. Zeng, A new configuration of winglet longitudinal vortex generator to enhance heat transfer in a rectangular channel, Appl. Therm. Eng. 104 (2016) 74–84, https://doi.org/10.1016/j.applthermaleng.2016.05.056.
[30] M. Fiebig, Vortices and Heat Transfer, ZAMM - J. Appl. Math. Mech. 77 (1) (1997) 3–18, https://doi.org/10.1002/zamm.19970770103.
[31] M. Fiebig, P. Kallweit, N. Mitra, S. Tiggelbeck, Heat transfer enhancement and drag by longitudinal vortex generators in channel flow, Exp. Therm. Fluid Sci. 4 (1) (1991) 103–114, https://doi.org/10.1016/0894-1777(91)90024-L.
[32] M. Vilarrubi, G. Laguna, A. Amnache, L.M. Collin, J.I. Rosell, M. Ibañez, J. Illa, L. G. Fréchette, J. Barrau, Thermostatic Fins for Spatially and Temporally Adaptive Microfluidic Cooling, in: THERMINIC 2018 -, 24th Int. Work. Therm. Investig. ICs Syst. Proc. (2018), https://doi.org/10.1109/THERMINIC.2018.8593306.
[33] M. Vilarrubí, J. Rosell, L.G. Fréchette, J. Barrau, Impact of thermally sensitive self-adaptive structures on the performance of a cooling device, in: Proc 30th Int. Conf. Adapt. Struct. Technol. ICAST 2019, International Conference on Adaptive Structures and Technologies, 2019, pp. 47–48.
[34] M. McCarthy, N. Tiliakos, V. Modi, L.G. Frechette, Temperature-regulated nonlinear microvalves for self-adaptive MEMS cooling, J. Microelectromechanical Syst. 17 (4) (2008) 998–1009, https://doi.org/10.1109/JMEMS.2008.927742.
[35] P.R. Champagne, A.E. Bergles, Development and testing of a novel, variable-roughness technique to enhance, on demand, heat transfer in a single-phase heat exchanger, J. Enhanc. Heat Transf. 8 (5) (2001) 341–352, https://doi.org/10.1615/JEnhHeatTransf.v8.i5.50.
[36] M.S. Aris, I. Owen, C.J. Sutcliffe, The development of active vortex generators from shape memory alloys for the convective cooling of heated surfaces, Int. J. Heat Mass Transf. 54 (15-16) (2011) 3566–3574, https://doi.org/10.1016/j.ijheatmasstransfer.2011.03.030.
[37] M. Vilarrubí, G. Morell, J. Rosell, L.G. Fréchette, J. Barrau, Experimental characterization of a self-adaptive shape memory alloy cooling approach to regulate temperature under varying heat loads, Int. J. Heat Mass Transf. 139 (2019) 632–640, https://doi.org/10.1016/J.IJHEATMASSTRANSFER.2019.05.028.
[38] A.C. Kneissl, E. Unterweger, G. Lojen, I. Anzel, Microstructure and Properties of Shape Memory Alloys, Microsc. Microanal. 11 (2005) 1704–1705, https://doi.org/10.1017/s1431927605500412.
[39] J.M. Company, Nitinol technical properties, Medical components resource library. (2021) 1.
[40] COMSOL Multiphysics, CFD Module - User's Guide, in: Comsol Multiphysics Manual, Version 5.3a, 2017: pp. 1–638.
[41] COMSOL Multiphysics, Heat Transfer Module - User's Guide, in: Comsol Multiphysics Manual, Version 5.3a, 2017: pp. 1–626.
[42] G. Costanza, M.E. Tata, C. Calisti, Nitinol one-way shape memory springs: Thermomechanical characterization and actuator design, Sensors Actuators, A Phys. 157 (1) (2010) 113–117, https://doi.org/10.1016/j.sna.2009.11.008.
[43] H.-C. Kim, Y.-I. Yoo, J.-J. Lee, Development of a NiTi actuator using a two-way shape memory effect induced by compressive loading cycles, Sensors Actuators, A Phys. 148 (2) (2008) 437–442, https://doi.org/10.1016/j.sna.2008.08.019.
[44] W. Huang, H.B. Goh, On the long-term stability of two-way shape memory alloy trained by reheat treatment, J. Mater. Sci. Lett. 20 (2001) 1795–1797, https://doi.org/10.1023/A:1012543402147.
[45] G. Eggeler, E. Hornbogen, A. Yawny, A. Heckmann, M. Wagner, Structural and functional fatigue of NiTi shape memory alloys, Mater. Sci. Eng. A. 378 (1-2) (2004) 24–33, https://doi.org/10.1016/j.msea.2003.10.327.